Supplementary Information

A validated method for contact angle measurement of low surface tension fluids using a modified Wilhelmy Plate Technique

Luca Fusina, Marco Tancon*, Fabio Casarin, Maria Basso, Elena Colusso,

Stefano Bortolin, Marco Azzolin

Department of Industrial Engineering, University of Padova,
Via Venezia 1, 35131 Padova, Italy

*Corresponding author:

Dr. Marco Tancon

Department of Industrial Engineering, University of Padova

Via Venezia 1, 35131 Padova, Italy

E-mail: marco.tancon@unipd.it

S1 Image analysis for contact angle determination

This Section describes the main steps for image analysis and the main parameters that must be set for accurate contact angle measurements. The evaluation of the Type B uncertainty through Monte Carlo simulations is also reported. The discussion is focused on the developed technique based on the modified Wilhelmy method, but similar considerations are also valid for the sessile drop method used during the validation phase. Specifically, a CMOS camera (Thorlabs GmbH® DCC1545M) coupled with a zoom lens (Thorlabs GmbH® MVL7000) was employed to measure contact angles with the sessile drop method, at ambient conditions. For dynamic sessile drop measurements, a precision syringe was used to expand and contract a droplet with a target volume of ~10 µL. To ensure quasi-static conditions and avoid inertial effects, the liquid was dispensed and withdrawn at a controlled average volumetric rate of ~1 µL s^{-1}, as performed in established literature protocols [1,2].

S1.1 Image analysis

The images from the high-speed camera are analyzed by means of a code developed in MATLAB® to retrieve the contact angle. The calculation of the contact angle is based on the intersection between the reference plane (the vertical wall of the cylinder) and the meniscus curve. The first step is the automatic subpixel detection of all the edges in the image, following the model proposed by Trujillo-Pino et al. [3] Next, it is possible to select a portion of the detected points lying on the wall edge and, by interpolation, the line representing the vertical wall is obtained. The method allows to account for small inclinations of the sample in the case it was not perfectly vertical. In a similar way, a portion of the points of the meniscus can be selected and interpolated, staying slightly away from the vertical wall [4]. From the equation of the wall line and the meniscus profile, their intersection point can be determined, as well as the tangent to the liquid-vapor interface at such point. The contact angle can be finally calculated as the angle between the tangent at the intersection point and the vertical line.

A similar code is also used for sessile drop measurements during the validation phase. In this case, the vertical wall identification is replaced by the determination of the horizontal baseline. The droplet profile is then fitted by a polynomial and the intersection between the interpolating curve and the horizontal baseline can be obtained. The contact angle is measured between the horizontal plane and the tangent to the drop's profile at the intersection point. The uncertainty in the identification of the contact angle from the pictures is estimated by means of Monte Carlo simulation in a similar manner to the modified Wilhelmy method, perturbing the horizontal plane instead of the vertical wall of the cylindrical samples.

S1.2 Effect of interpolating polynomial degree

As a general rule, when interpolating the meniscus, a single polynomial degree is not suited for all the angles to be measured. In fact, as the angle varies, a different polynomial degree should be chosen. The very last portion of the meniscus closer to the vertical wall should not be selected for the interpolation, due to unclear detection of the intersection of the two lines especially at low contact angles [4]. Therefore, the polynomial should be capable of some extrapolation. As the degree increases, lower angles can be detected (whereas lower degrees tend to overestimate the contact angle), but extrapolation becomes more difficult with possible fluctuations of the polynomial outside the domain of interpolation. Hence, a compromise is required, to optimize the choice of the degree, and some guidelines are crucial for accurate measurements.

Table S1 reports the angles resulting from the measurement procedure with some polynomial degrees chosen as examples. Three cases are considered, with decreasing angle from case 1 to case 3, approximately 48°, 32° and 7°, respectively. In case 1, where the angle is relatively high, moving from degree 2 to degree 8 leads to a difference of about 3° (that is, 6.1%). In case 3, however, the difference is over 9°. This variability is clearly unacceptable.

Table S1. Effect of the interpolating polynomial on the contact angle measurement, for three cases in the range 0°–90°.

Polynomial degree	Case 1	Case 2	Case 3
2	48.6°	33.5°	16.5°
3	48.1°	32.2°	12.3°
4	47.4°	32.4°	9.9°
5	47.8°	32.4°	8.5°
6	46.7°	31.5°	7.5°
8	45.7°	27.6°	6.8°

As expected, if the angle is high enough, a low degree provides a more stable solution. On the contrary, higher degrees can be better for lower angles, since they allow to better follow the steep rise of the meniscus. Nevertheless, with a high polynomial degree only a small portion of the liquid-vapor interface can be accurately described. A more quantitative approach is described hereafter. Fig. S1a refers to case 3, where, by comparison with the original image, it can be observed that the angle is below 10°. It reports the error in pixels, calculated as difference between the detected interface points and the corresponding points of the interpolating polynomial, at common horizontal coordinates (as illustrated in Fig. S1b). Note that the horizontal image coordinate approaches the wall towards the right. Different polynomial degrees are considered. One can see that with a higher degree, the error close to the vertical wall is lower. It must be observed that the last few pixels closest to the wall should not be considered because the interface is generally not clear and blurred, as already mentioned. Therefore, the comparison between interpolation and detected points at the liquid-vapor interface

should not include the last couple of pixels in the graph. It results that a polynomial of degree equal to 6 gives an error consistently below 1 pixel in the entire region that can be analyzed.

In general, it is always essential to compare the polynomial curve with the original image, to check deviations which are merely caused by an inappropriate interpolation. In fact, if too many or not enough points are selected for the interpolation, the resulting curve might behave poorly.

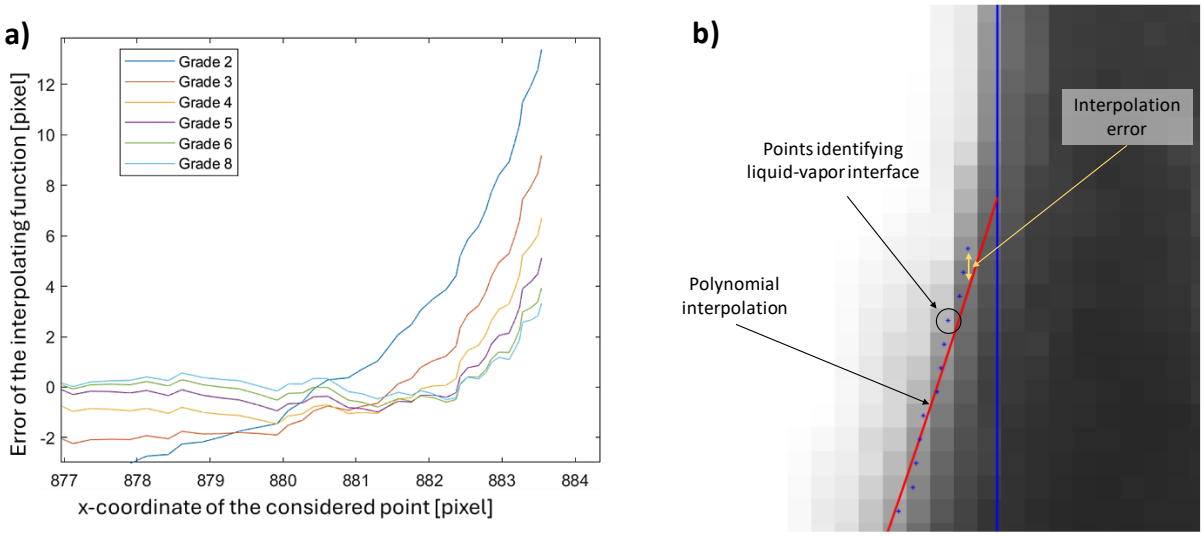

Fig. S1. a) Effect of the interpolating polynomial degree on the error between the points detected on the meniscus and the points obtained from the polynomial, against the horizontal coordinate (the vertical wall is towards the right), for a reference angle below 10° (case 3). b) Example of calculation of the error between the interpolating polynomial and the points at the interface identified by image analysis.

S1.3 Effect of the number of interpolated points at the meniscus

The length of the portion of the meniscus selected for analysis is another crucial aspect. This choice must be made considering the chosen degree of the polynomial, as they are connected. Fig. S2 reports the trend of contact angle against the number of interpolated points. The rightmost point, which is the closest to the cylinder wall, is fixed, and other points are progressively included, from right to left. In fact, excluding the points close to the wall would result in obviously higher errors. At least ten points are always considered. Two scenarios are analyzed with four different polynomial degrees between 2 and 8, the first with an angle of 32° (case I), and the second with an angle of 5° (case II).

In both cases of Fig. S2, there are strong fluctuations of the contact angle when few points are added or excluded, if the number of total points is low, and higher instability is observed with higher degree polynomials. For relatively high contact angles, as in case I, low degrees of polynomials (between 2 and 4) are considered the most suitable, requiring at

least 40 points to become approximately independent of the number of points, whereas around 30 points are enough in case II, with degree above 4 (the variation of θ with the number of interpolated points becomes lower than the expanded uncertainty of the measurements). Low-degree polynomials, on the other hand, tend to overestimate low contact angles, in any situation. Finally, an increasing trend of the contact angle against the number of interpolated points emerges clearly in Fig. S2b. Indeed, including an excessive number of points far from the meniscus makes the polynomial flatter, with higher deviation from the real capillary rise at the solid interface.

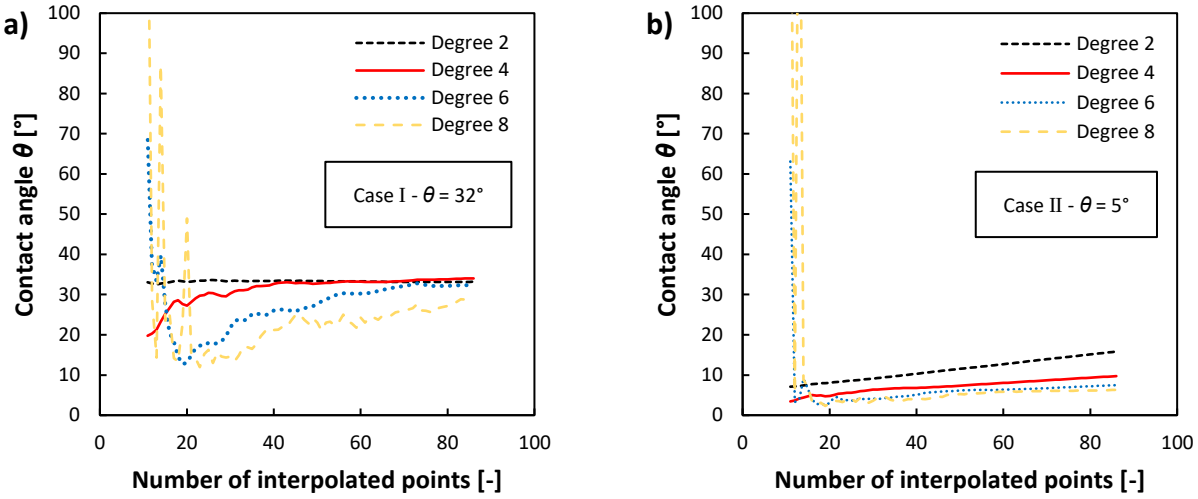

Fig. S2. Effect of the number of the points considered for the interpolation on the resulting contact angle, for four polynomial degrees, namely 2, 4, 6, and 8, for the images of case I (a) and case II (b). The rightmost points of the selected portion of the meniscus, which are closer to the cylinder wall, are always considered, and additional points are progressively included on the left side, where the meniscus becomes flatter.

To conclude, contact angle evaluation requires careful consideration of all the parameters discussed above, including polynomial degree, number of interpolated points, and interpolation range. Their optimal choice depends on the approximate value of the target angle and the specific experimental conditions. In terms of reliability, the method is highly robust for contact angles above 20°, where the sensitivity to parameter selection within the suggested ranges is minimal and the resulting variability is typically lower than 0.8°. Particular attention should be paid to angles below 20° (and especially below 10°), where the choice of parameters becomes more critical due to the steep meniscus curvature. As a general guideline, polynomial degrees of 3 – 4 are suitable for contact angles > 10°, whereas higher degrees (6 – 8) are recommended for angles < 10°, together with an adequate number of interpolation points. Different parameter combinations should be systematically compared to identify the most appropriate conditions, always ensuring consistency with the original image. In this context, the procedure should not be regarded as purely trial-and-error, but rather as a

guided and quantitative approach, in which the influence of parameters is explicitly assessed. The use of quantitative metrics, such as interpolation error, further supports the selection of optimal conditions, enabling more accurate and reliable contact angle determination.

S1.4 Type B uncertainty estimation from Monte Carlo simulations

The Type B uncertainty was estimated from simulations in which the points of the vertical sample wall and the points of the meniscus were perturbed randomly (by 1 pixel). For each case (2×10^5 simulations), a standard deviation $\sigma_{N,MC}$ was calculated. An average value was then extracted from $\sigma_{N,MC}$ of several simulations with different contact angles in the range 0° – 90°. This value, equal to 0.5°, was therefore considered as Type B uncertainty, u_B. As in Fig. S3, $\sigma_{N,MC}$ is independent of the contact angle, justifying a constant u_B for all the images.

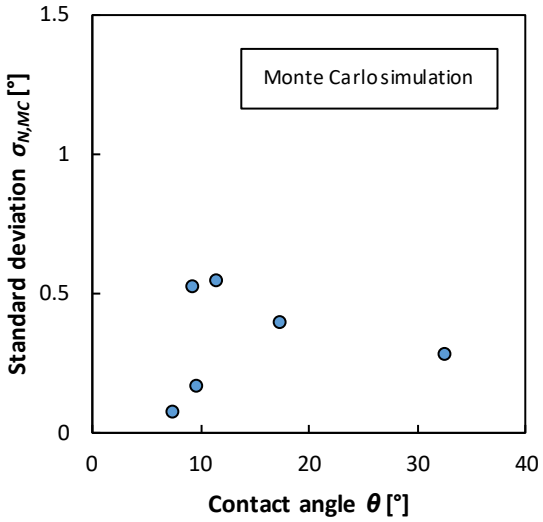

Fig. S3. Standard deviation of the contact angle obtained from Monte Carlo simulations by perturbing the wall and liquid-vapor interface points by 1 pixel for different values of contact angle.

S2 Results of validation

Three fluids are used for validation, namely water, ethylene glycol and ethanol. Tests were carried out at ambient conditions. The results of the validation with static contact angles on aluminium, copper, PTFE, M7T3, and O2T8 samples are reported in Table S2. For sessile drop tests, the samples are flat, while the samples are cylindrical for tests with the present modified Wilhelmy method.

Table S2. Comparison of static contact angles θ_s measured by standard sessile drop and present methods, with the experimental uncertainty calculated following the procedure described in Section "Data reduction and uncertainty analysis" of the manuscript. The values for water on PTFE and O2T8 are omitted because the present setup cannot accurately determine angles above 90°.

Surface	Method	Water	Ethylene glycol	Ethanol
Aluminium	Sessile	64.4° ± 3.7°	48.5° ± 5.8°	10.6° ± 5.9°
	Present method	68.3° ± 1.9°	49.1° ± 2.0°	10.3° ± 1.9°
Copper	Sessile	59.3° ± 3.3°	43.9° ± 1.0°	9.3° ± 3.3°
	Present method	59.6° ± 4.8°	43.6° ± 1.5°	7.8° ± 1.6°
PTFE	Sessile	104.4° ± 3.1°	82.5° ± 2.3°	48.0° ± 1.8°
	Present method	-	79.1° ± 1.6°	48.7° ± 3.3°
M7T3	Sessile	79.9° ± 3.5°	57.1° ± 3.0°	12.4° ± 3.0°
	Present method	80.2° ± 2.1°	56.6° ± 1.7°	10.0° ± 1.3°
O2T8	Sessile	93.0° ± 4.0°	72.0° ± 1.4°	18.2° ± 2.8°
	Present method	-	73.1° ± 1.2°	20.1° ± 2.1°

Dynamic contact angles were measured at ambient temperature (20 °C) and at constant immersion and withdrawal velocity of 0.05 mm s^{-1}. An aluminium substrate with the M7T3 coating was used for validation, with the three fluids. Results are reported in Table S3.

Table S3. Comparison of dynamic and static contact angles on the M7T3 sample, measured by standard sessile drop and present methods, with the experimental uncertainty calculated following the procedure described in Section "Data reduction and uncertainty analysis" of the manuscript.

Fluid	Method	θ_a	θ_r	θ_s
Water	Sessile	80.3° ± 2.7°	61.1° ± 2.1°	79.9° ± 3.5°
	Present method	80.4° ± 1.0°	60.3° ± 1.6°	80.2° ± 2.1°
Ethylene glycol	Sessile	64.5° ± 2.6°	36.7° ± 3.4°	57.1° ± 3.0°
	Present method	61.9° ± 1.4°	36.8° ± 1.3°	56.6° ± 1.7°
Ethanol	Sessile	19.7° ± 4.8°	6.5° ± 1.1°	12.4° ± 3.0°
	Present method	16.8° ± 3.3°	7.2° ± 1.3°	10.0° ± 1.3°

S3 Contact angle measurements with refrigerants R1234ze(E) and R1233zd(E)

The wettability of two refrigerants with normal point below ambient temperature, R1234ze(E) and R1233zd(E), was experimentally investigated with the setup described in Section "Experimental setup for the optical modified Wilhelmy method" of the manuscript, under saturated conditions. For R1234ze(E), an aluminium sample was tested as reference. Then, the PTFE and O2T8 samples were tested with both R1234ze(E) and R1233zd(E). The contact angles of R1234ze(E) and R1233zd(E) are reported in Table S4 and Table S5, respectively. An example of contact angles of refrigerant is illustrated in Fig. S4, for R1233zd(E) on the O2T8 coated aluminium substrate.

Table S4. Static and dynamic contact angles of R1234ze(E) on aluminium, PTFE, and O2T8 cylinders.

Surface	θ_a	θ_r	θ_s
Aluminium	5.6° ± 1.0°	2.3° ± 1.2°	5.3° ± 1.4°
PTFE	8.1° ± 1.1°	5.3° ± 1.0°	6.7° ± 1.7°
O2T8	8.7° ± 1.1°	5.4° ± 1.2°	7.4° ± 1.0°

Table S5. Static and dynamic contact angles of R1233zd(E) on PTFE and O2T8 cylinders.

Surface	θ_a	θ_r	θ_s
PTFE	7.2° ± 1.5°	4.0° ± 1.0°	6.4° ± 1.1°
O2T8	8.3° ± 1.2°	5.9° ± 1.4°	6.3° ± 1.1°

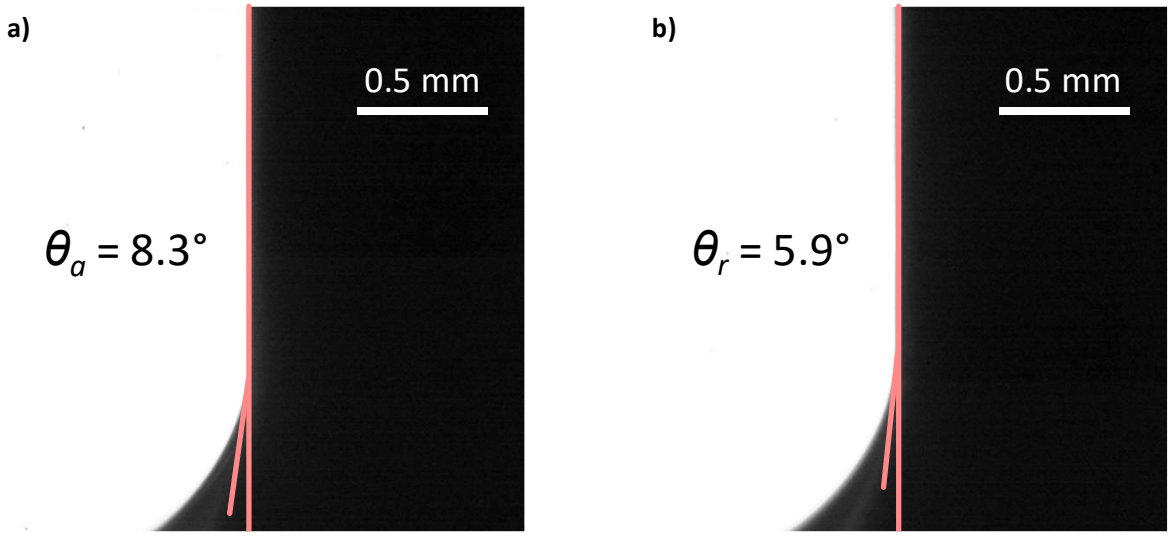

Fig. S4. Visualizations of advancing (a) and receding (b) contact angles of R1233zd(E) on O2T8 sol-gel coated aluminium sample.

S4 Surface energy determination

The OWRK method is based on the interaction of at least two probe solvents with different polarities on the surface, such as water, ethylene glycol and diiodomethane. For each solvent, the experimental static CA (θ), the surface tension of the probe solvent (γ_l), the polar (γ_l^p) and the disperse (γ_l^d) component of the solvent are required parameters for the assessment of the surface energy of the coating. For the selected solvents, γ_l, γ_l^p, γ_l^d, are tabulated values and reported in Table S6, while contact angles are measured with the sessile drop method.

Table S6. Surface energy data determined at 25°C.

	Aluminum	**PTFE**	**O2T8**	**M7T3**	**Literature**			
Solvent	θ_s	θ_s	θ_s	θ_s	**γ_l [mJ/m^2]**	**γ_l^p [mJ/m^2]**	**γ_l^d [mJ/m^2]**	**Ref**
Water	64.4° ± 3.7°	104.4° ± 3.1°	93.0° ± 4.0°	79.9° ± 3.5°	72.8	45.61	27.19	[5,6]
Ethylene glycol	48.5° ± 5.8°	82.5° ± 2.3°	72.0° ± 1.4°	57.1° ± 3.0°	48	18.19	29.81	[6]
Diiodo methane	43.6° ± 1.9°	85.5° ± 2.1°	62.3° ± 2.1°	54.5° ± 1.0°	50.8	1.8	49	[7]

The surface energy of the solid is calculated by fitting the experimental CA and the polar and dispersed component of the probes according to the equation:

$$\gamma_s = \gamma_s^p + \gamma_s^d \quad \text{(S1)}$$

The relation among the two components of surface energy (γ_s^p, γ_s^d), solvent surface tension (γ_l^p, γ_l^d), and the contact angle can be expresses in a linear form as follows [8]:

$$y = mx + q \quad \text{(S2)}$$

$$\text{where } y = \frac{1}{2}\frac{(1+\cos\theta)\gamma_l}{\sqrt{\gamma_l^d}} \quad \text{(S3)}$$

$$x = \sqrt{\frac{\gamma_l^p}{\gamma_l^d}} \quad \text{(S4)}$$

$$q = (\gamma_s^d)^{1/2} \quad \text{(S5)}$$

$$m = (\gamma_s^p)^{1/2} \quad \text{(S6)}$$

A graphical representation of the OWRK method is shown in Figure S5 for the O2T8.

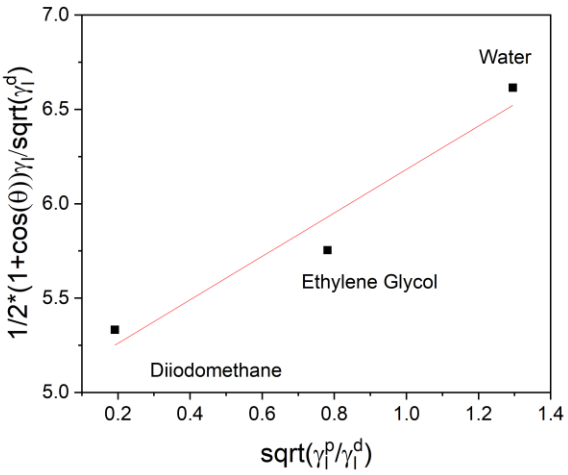

Fig. S5. A representative surface energy (polar and dispersive) calculation graph based on OWRK model for O2T8 sample.

Table S7. Fitting data of surface energy

	Aluminum	**PTFE**	**O2T8**	**M7T3**
q **[mJ/m^2]$^{1/2}$**	5.33	3.88	5.03	5.26
m **[mJ/m^2]$^{1/2}$**	3.27	1.24	1.15	2.19
R^2	0.92	0.92	0.95	0.98
γ_s [mJ/m^2]	39.1	16.6	26.6	32.5

References

1. Li, S. *et al.* Durable, Ultrathin, and Antifouling Polymer Brush Coating for Efficient Condensation Heat Transfer. *ACS Appl. Mater. Interfaces* **16**, 1941–1949 (2024).
2. Lam, C. W. E. *et al.* Condensate droplet roaming on nanostructured superhydrophobic surfaces. *Nat. Commun.* **16**, 1167 (2025).
3. Trujillo-Pino, A., Krissian, K., Alemán-Flores, M. & Santana-Cedrés, D. Accurate subpixel edge location based on partial area effect. *Image Vis. Comput.* **31**, 72–90 (2013).
4. Lu, X., Liu, J. & Xu, X. Contact angle measurements of pure refrigerants. *Int. J. Heat Mass Transf.* **102**, 877–883 (2016).
5. Morita, M., Ohmi, T., Hasegawa, E., Kawakami, M. & Ohwada, M. Growth of native oxide on a silicon surface. *J. Appl. Phys.* **68**, 1272–1281 (1990).
6. Zdziennicka, A., Krawczyk, J., Szymczyk, K. & Jańczuk, B. Components and parameters of liquids and some polymers surface tension at different temperature. *Colloids Surf. A Physicochem. Eng. Asp.* **529**, 864–875 (2017).
7. Fernández, V. & Khayet, M. Evaluation of the surface free energy of plant surfaces: Toward standardizing the procedure. *Front. Plant Sci.* **6**, 510 (2015).
8. Annamalai, M. *et al.* Surface energy and wettability of van der Waals structures. *Nanoscale* **8**, 5764–5770 (2016).